Surface hopping within an exciton picture -

An electrostatic embedding scheme

Maximilian F.S.J. Menger,[†,‡] Felix Plasser,[*,†,¶] Benedetta Mennucci,[*,‡] and Leticia González [*,†]

†Institute for Theoretical Chemistry, Faculty of Chemistry, University of Vienna, Währingerstr. 17, 1090 Vienna, Austria

‡Dipartimento di Chimica e Chimica Industriale, University of Pisa, Via G. Moruzzi 13, 56124 Pisa, Italy

¶Department of Chemistry, Loughborough University, Loughborough LE11 3TU, U.K.

E-mail: felix.plasser@univie.ac.at; benedetta.mennucci@unipi.it; leticia.gonzalez@univie.ac.at

Abstract

We report the development and the implementation of an exciton approach that allows the computing of ab initio non-adiabatic dynamics simulations of electronic excitation energy transfer in multichromophoric systems. For the dynamics a trajectory based strategy is used within the surface hopping formulation. The approach features a consistent hybrid formulation that allows the construction of potential energy surfaces and gradients by combining quantum mechanics and molecular mechanics within an electrostatic embedding scheme. As an application, the study of a molecular dyad consisting of a covalently bound BODIPY moiety and a tetrathiophene group is also presented using time-dependent density functional theory (TDDFT). The results obtained with the exciton model are compared to previously performed full TDDFT dynamics of the same system. Our results show excellent agreement with the full TDDFT results indicating that the couplings that lead to excitation energy transfer (EET) are dominated by Coulomb interaction terms and that charge transfer states are not necessary to properly describe the non-adiabatic dynamics of the system. The exciton model also reveals ultrafast coherent oscillations of the excitation between the two units in the dyad, which occur during the first 50 fs.

1 Introduction

Electronic excitation energy transfer is a fundamental process observed in biosystems and materials through which an excited chromophore (the donor) nonradiatively transfers the excitation energy to a proximate chromophore (the acceptor). One of the most prominent example of this process is the initial step of photosynthesis, where the excitation energy is transferred many times within and between pigment-protein complexes until the reaction center is reached.[1,2] Other applications of EET processes in biosystems are in the mechanisms of photoreceptors[3,4] or DNA photodamage.[5,6] Additionally EET processes are often used to study the structure and dynamics in complex molecular systems, where the EET efficiency is strongly sensitive to the distance and to the relative orientation of the donor and acceptor moieties.[7]

The theoretical investigation of EET processes can be highly challenging due to (i) the size of the system, (ii) the influence of the environment and (iii) the involved nonadiabatic dynamics. To address problem (i) approximate methods have been developed which avoid the computation of the full system quantum mechanically; even computationally effective methods like TDDFT can in fact become unfeasible for large multichromophoric aggregates. Among these approximate methods, the Frenkel exciton model represents a very effective one.[8] Hereby, the Hamiltonian of the whole system is rewritten in terms of a model Hamiltonian, whose elements can be obtained from calculations on the individual chromophores, thus reducing the computational costs significantly and allowing to treat much larger systems. In the Frenkel exciton model the diagonal elements of the model Hamiltonian are the excitation energies of the individual chromophores, the so-called *site energies*, while the off-diagonal elements are the *excitonic coupling* between these local excitations. When the latter correspond to "bright" states and there is no significant overlap of the corresponding wavefunctions, the dominant term is the Coulombic interaction between the transition

densities of the donor and acceptor moieties, namely.[9,10]

$$V_{DA}^{IJ} = \int dr \int dr' \rho_D^{T*}(r') \frac{1}{|r - r'|} \rho_A^T(r) \qquad (1)$$

Eq. (1) can be evaluated either by analytical integration techniques[11,12] or by numerical integration after discretizing the integral in terms of a sum over finite sized volume elements.[13] Alternatively, the transition densities in Eq. (1) can be approximated using distributed atom-centered transition monopoles (transition charges). Various definitions of the atomic transition charges have been proposed so far[14,15] including the very effective one based on the fitting to the electrostatic potential generated by the transition density,[16] as it is typically done to parametrize point charge models in biomolecular force fields. Another, very popular method to obtain the coupling, goes back to the work of Förster 70 years ago[17] and uses a point dipole approximation (PDA) reducing the transition densities to transition dipoles.

Moving to problem (ii), extensions of the exciton model to include electrostatic and polarizable embedding schemes have been presented, using both discrete and implicit solvation.[11,12,18,19] Electrostatic embedding has a direct effect only on the site energies whereas polarizable embedding schemes can also directly influence the couplings through dielectric screening of the Coulomb interaction,[18,20–22] and the latter can effect the EET rates significantly.[23]

Finally, to address challenge (iii), the most common formulation of EET dynamics is based on the assumption of excitations being localized on one or a few chromophores at a time, while energy transfer occurs via a hopping mechanism between chromophores. Within this assumption, the perturbative Golden Rule expression proposed by Förster can be effectively used, which gives an expression for the energy transfer rate for each donor and acceptor pair, as

$$k_{EET} = \frac{2\pi}{h} |V_{DA}|^2 \text{FCWD} \qquad (2)$$

where FCWD is the Franck-Condon factor weighted density of states expressed as the spectral

overlap of the two separate FCWD functions of donor and acceptor.[24] When the electronic coupling between donor and acceptor is large, such an expression is not valid anymore, as the electronic coupling tends to delocalize the excitation over both chromophores, giving rise to exciton states.[25] In multichromophoric systems as DNA or light-harvesting pigment-protein complexes, the excitation may be shared among several chromophores.[26] Within this strong coupling regime, the excited-state dynamics consists in intraband relaxation between exciton states and an effective approach to describe such relaxation is represented by Redfield theory.[27,28] In both these alternative formulations, a perturbative treatment is used, where either the electronic coupling or the coupling of the electronic process to vibration is the perturbation.[29] Only more recently, an explicit treatment of non-adiabatic dynamics was addressed by Martínez and coworkers by combining an exciton model with non-adiabatic surface hopping dynamics.[30,31] Going further along the same line, this work presents a combination of surface hopping non-adiabatic dynamics with an exciton model that includes the interaction between the chromophores (and an eventual external environment) through an hybrid QM/MM formulation with an electrostatic embedding scheme and describes excitonic couplings using atom centered transition charges instead of point dipoles. Consistent expressions for the potential energy surfaces, their gradients and non-adiabatic couplings have been developed and implemented in an exciton package utilizing the Gaussian suite of codes[32] for the electronic structure calculations. The resulting exciton package has finally been interfaced with the SHARC (Surface Hopping including ARbitrary Couplings) code[33–35] to perform the non-adiabatic dynamics simulations.

As a test case we study the EET dynamics within a molecular dyad (BODT4) which consists of a boron dipyromethene dye (BOD) and a tetrathiophene (T4) unit (see Fig. 1). The recently measured time-resolved photoluminescence spectrum of the system indicates an energy transfer process completed within a sub-picoscecond timescale.[36] This experimental result was interpreted with the help of surface hopping dynamics study on the full system, as an ultrafast excitation energy transfer from the T4 moiety to the BOD fragment which
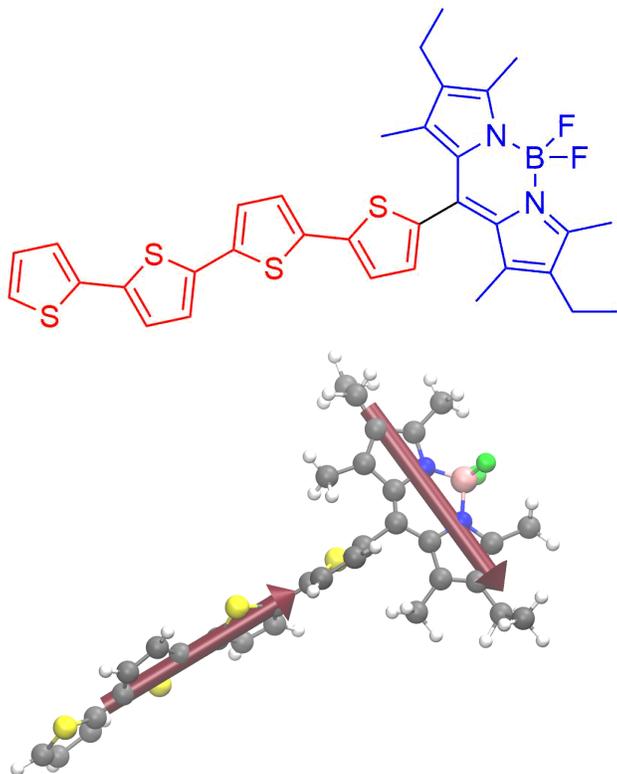
Figure 1: (Upper panel: BODT4 molecular structure underlying T4 (red) and BOD (blue) moieties. Lower panel: 3D representation of the system with the corresponding transition dipoles of the S_1 state of the BOD and T4 groups centered at the center of mass of the moieties.

occurs through an intermediate charge-transfer state. The excellent agreement of our exciton model with these previous results, however, seems to indicate that the couplings that lead to the energy transfer are dominated by Coulomb interactions and that charge transfer effects are not necessary to obtain the same non-adiabatic dynamics. The present exciton model also reveals ultrafast coherent oscillations of the excitation between the two units in the dyad, which occur during the first 50 fs.

2 Theory

Trajectory surface hopping has become an important tool to study non-adiabatic dynamics for medium sized systems.[37] It combines a classical treatment of the nuclei, a quantum mechanical description of the electrons, and a semi-classical treatment of their interactions. In the original Tully's fewest switches surface hopping formulation, three main ingredients are needed, namely (i) the energies of the electronic states, (ii) the corresponding gradients and (iii) the nonadiabtic couplings (NACs) between the states.[34] In typical surface hopping implementations, the required information is directly calculated for the full system with the help of an electronic structure program.[34,38] Here, we proceed in a different way. First, the electronic structure computations are performed for each chromophore. Subsequently, these results are combined using a Frenkel exciton model approach to compute the energies, gradients, and non-adiabatic couplings for the whole system.

2.1 Excitation Energies in the Exciton Model

Within the diabatic basis of locally excited states the excitonic Hamiltonian H^{ex} is written as:

$$\hat{H}^{ex} = \sum_{\alpha} \sum_{I}^{N(\alpha)} \Omega_{\alpha}^{I} |\alpha I\rangle\langle\alpha I| + \sum_{\alpha,\beta\neq\alpha} \sum_{I}^{N(\alpha)} \sum_{J}^{N(\beta)} V_{\alpha\beta}^{IJ} |\alpha I\rangle\langle\beta J| \tag{3}$$

In this notation α and β refer to different individual chromophores while I and J mark specific excited states on these chromophores. Ω_{α}^{I} is the excitation energy of the Ith locally excited state on chromophore α, the so-called site energy, and $V_{\alpha\beta}^{IJ}$ is the excitonic coupling between two states on different chromophores.

The site energies Ω_{α}^{I} are obtained as excitation energies by standard quantum chemistry computations, using in the present case TDDFT. In the case of "bright" singlet states, which are the focus of this work, it is possible to approximate the excitonic coupling elements through the Coulomb interaction between transition densities,[10] cf. Eq. (1). If however, we introduce the already cited PDA, the excitonic coupling can be reduced to the interaction

between corresponding transition dipoles $\vec{\mu}_{\alpha I}$, namely

$$V_{\alpha\beta}^{IJ,(PDA)} = \vec{\mu}_{\alpha I} \cdot \vec{\mu}_{\beta J} - \frac{3(\vec{R}_{\alpha\beta} \cdot \vec{\mu}_{\alpha I})(\vec{R}_{\alpha\beta} \cdot \vec{\mu}_{\beta J})}{|\vec{R}_{\alpha\beta}|^2} \qquad (4)$$

where $\vec{R}_{\alpha\beta}$ is the vectorial distance between the transition dipoles on the chromophores α/β. The PDA works well if the distance between the involved chromophores is larger than the spatial dimension of the chromophores,[10,17] but can break down for short inter-chromophoric distances. As an alternative to the PDA method, we use here the so-called transition monopole approximation (TMA) based on the TrESP charges, that were obtained from electrostatic potential fitting.[16] Using TrESP charges, Eq. (1) can be approximated as:

$$V_{\alpha\beta}^{IJ,(TMA)} = \sum_{K,L} \frac{q_\alpha^I(K)q_\alpha^J(L)}{R_{KL}}, \qquad (5)$$

with $q_\alpha^I(K)$ being the TrESP charge localized at atom K on chromophore α and obtained by the electrostatic potential fitting of the transition density $\rho_{\alpha I}$. In the following the TMA is always used with TrESP charges and therefore TMA couplings and TrESP coupling have the same meaning.

Once the exciton matrix is constructed, one obtains the excitation energies ω_j of the multichromophoric system as the eigenvalues of the matrix representation of $\hat{H}^{ex}$

$$\begin{pmatrix} \omega_1 & 0 & 0 \\ 0 & \omega_2 & 0 \\ 0 & 0 & \ddots \end{pmatrix} = \mathbf{U}^\dagger \mathbf{H}^{ex} \mathbf{U} \qquad (6)$$

where $\mathbf{U}$ is the transformation matrix that diagonalizes the exciton Hamiltonian.

2.2 Ground state and Gradients in the Exciton Model

Whereas the computation of vertical excitation energies within an exciton model is already well established,[10] it is significantly more challenging to formulate a consistent hybrid model for computing the overall potential energy surfaces and their gradients. The reason for this is that in the former case the number of terms to consider is significantly reduced, as all terms relating to the ground state cancel out. If the ground state energy $\mathcal{E}_0$ is also considered, the total Hamiltonian matrix is written as:

$$\mathbf{H} = \mathcal{E}_0 \mathbf{1} + \begin{pmatrix} 0 & 0 \\ 0 & \mathbf{H}^{ex} \end{pmatrix} \tag{7}$$

using the exciton Hamiltonian matrix defined above to express the excited state contributions. The ground state shifts the eigenvalues of the matrix but does not affect the eigenvectors. Thus, it can be considered separately in the following discussion.

Generally, we follow the idea of a subtractive QM/MM scheme based on ONIOM.[39,40] For one chromophore, this consists of three basic steps: (i) a MM calculation of the whole system, (ii) a QM calculation of the chromophore, and (iii) a MM calculation of the chromophore that is subtracted to avoid double counting. In the case of multiple chromophores one can employ a similar strategy if only mechanical embedding is employed. In this case, the energy can be computed as

$$\mathcal{E}_0^{mech} = E_S^{MM} + \sum_{\alpha} (E_{\alpha}^{0,gas} - E_{\alpha}^{MM}) \tag{8}$$

In Eq. (8), the first term E_S^{MM} is the energy of the total system computed at MM level and the second is the sum over all chromophores α considering the difference between their QM ground state energy $E_{\alpha}^{0,gas}$ and MM energy E_{α}^{MM}.

The case of electrostatic embedding is significantly more challenging as new interaction terms come into play and one has to assure that each of these terms is counted exactly once. As shown in Fig. 2, three different types of electrostatic interaction terms come into

play: the interaction of the chromophores with the environment ($\varepsilon_{\alpha,env}$), interchromophore interactions ($\varepsilon_{\alpha,\beta}$), and interactions within the environment ($\varepsilon_{env,env}$). Whereas all these terms are included in E_S^{MM} of the mechanical embedding scheme, it is necessary to treat them individually for electrostatic embedding. As a starting point, an electrostatic embedding computation of an individual chromophore, as illustrated in Fig. 2 (d), is discussed. Here chromophore α is treated at the QM level while the environment and all other chromophores are represented by point charges.

$$E_\alpha^{0,ele} = \varepsilon_\alpha^0 + \sum_{\beta \neq \alpha} \varepsilon_{\alpha(QM),\beta(MM)}^0 + \varepsilon_{\alpha(QM),env} \tag{9}$$

The three terms represent the energy of the electrons within chromophore α, their interactions with other chromophores and with the environment, respectively. An electrostatic embedding calculation of a second chromophore β is illustrated in Eq. (8) (e). Whereas this calculation correctly introduces the new terms ε_β^0 and $\varepsilon_{\beta(QM),env}$, it also includes the interchromophore interaction through the term $\varepsilon_{\alpha(MM),\beta(QM)}^0$. Thus, the interchromophore interaction is included in both QM/MM calculation and would be counted twice if Eq. (8) was simply applied to the case of electrostatic embedding.

Following the philosophy of subtractive QM/MM schemes, we solve this problem by approximating the electrostatic interaction energy between the two chromophores as:

$$\varepsilon_{\alpha,\beta} \approx \varepsilon_{\alpha(QM),\beta(MM)} + \varepsilon_{\alpha(MM),\beta(QM)} - \varepsilon_{\alpha(MM),\beta(MM)} \tag{10}$$

The last term (shown in Fig. 2 (f)) is a correction based on the classical electrostatic interactions between the two chromophores α and β using their MM point charges. Applying this approximation the exciton ground state energy of a multichromophoric system can be
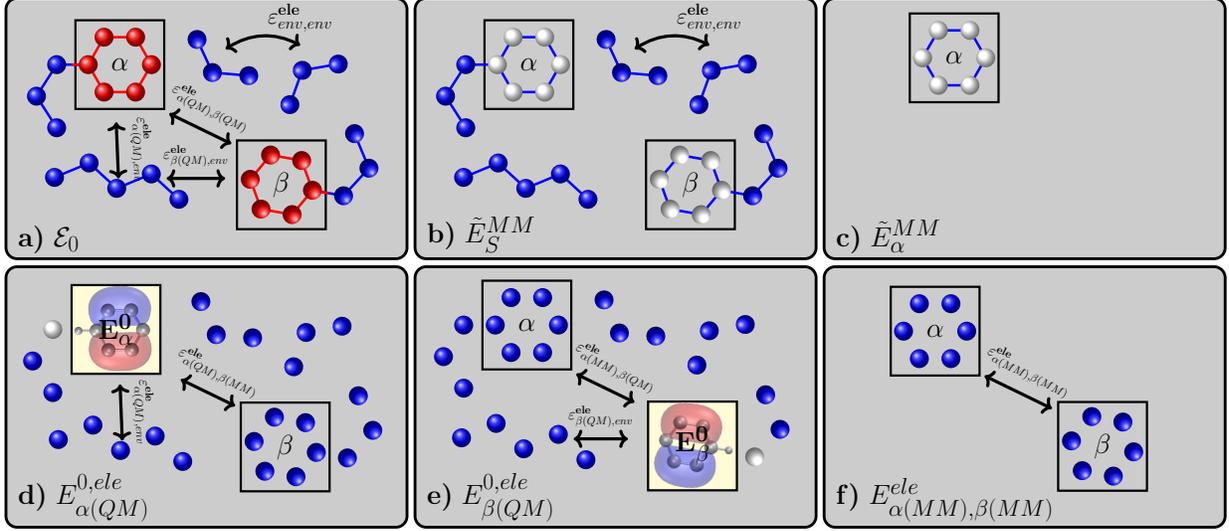
Figure 2: Sketch of a multichromophoric system with two chromophores (red) and an environment (blue). The electrostatic interactions are shown with arrows. In (a) the total system is shown. The MM energy of the total system is shown in (b), here blue atoms indicate that a MM charge is included in the computation while white indicates that it is set to zero. The contribution of the QM region treated at MM level of theory is shown in (c), again all MM charges of the QM region are set to zero. Panels (d) and (e) represent the electrostatic embedding calculations of the two individual chromophores where the QM region is represented as an orbital while point charges are shown in blue. Panel (f) represents the MM electrostatic interaction of the two chromophores that is subtracted to avoid double counting.

rewritten as:

$$\mathcal{E}_0^{ele} = \tilde{E}_S^{MM} - \sum_\alpha \tilde{E}_\alpha^{MM} + \sum_\alpha \left(E_\alpha^{0,ele} - \sum_{\beta > \alpha} E_{\alpha(MM),\beta(MM)}^{ele} \right) \tag{11}$$

where $\tilde{E}_S^{MM}$ is the MM energy of the total system without electrostatic interactions of the chromophores with the environment and among themselves, as already computed in the QM calculations. This is realized by setting the charges on the MM sites of the chromophores to zero in the MM calculations. The same holds for $\tilde{E}_S^{MM}$. Thus, in agreement with other subtractive QM/MM approaches for electrostatic embedding like the ONIOM scheme,[39,40] we add the electrostatic QM/MM interaction in the QM calculation $E_\alpha^{0,ele}$, while all non-electrostatic interactions are computed classically in the MM terms ($\tilde{E}_S^{MM}, \tilde{E}_\alpha^{MM}$). All terms

11

of Eq. (11) are shown in Fig. 2 for a system consisting of two chromophores.

Once the ground state energy is defined, it is straightforward to formulate its analytic gradient. Subsequently, the excited-state gradients can be computed as the sum of the gradient of the ground state and the gradient of the excitation energy.

$$\mathcal{E}_j^{\xi} = \mathcal{E}_0^{\xi} + \omega_j^{\xi} \tag{12}$$

Here, the excitation energies ω_i of the multichromophoric system are obtained by solving Eq. (6) and the gradient of the excited state can be expressed in terms of the derivative of the elements of the exciton Hamiltonian:

$$\begin{pmatrix} \omega_1^{\xi} & 0 & 0 \\ 0 & \omega_2^{\xi} & 0 \\ 0 & 0 & \ddots \end{pmatrix} = \mathbf{U}^{\dagger} \mathbf{H}^{ex,\xi} \mathbf{U} \tag{13}$$

The derivative of the excitonic coupling elements are straight forward if the TMA (PDA) approximation is used and only the Hellmann-Feynman forces are considered, which assumes that the TrESP (TrDip) remain constant in the gradient calculation. The gradients of the site energies ($H_{\alpha I,\alpha I}^{ex} = \Omega_\alpha^I$) can be obtained from the quantum chemistry calculation as the difference between the gradient of the excited state I and the ground state gradient of chromophore α.

2.3 Non-adiabatic couplings

Besides the gradients also non-adiabatic couplings are required for surface hopping. In this implementation we approximate them with a wavefunction overlap,[41–45] as it is implemented in the SHARC code[35]. For the overlap computation the algorithm and the code presented in Ref. 45 are used. Within this formulation, the non-adiabatic couplings are computed as the wavefunction overlaps between two consecutive time steps:

$$S_{ij}(t, t + \Delta t) = \langle \Psi_i | \tilde{\Psi}_j \rangle \tag{14}$$

with Ψ_i being the excited state wavefunction at time t of state i and $\tilde{\Psi}_j$ being the excited state wavefunction of state j, the tilde is used to indicate the wavefunction at the consecutive time steps $t + \Delta t$.

Within the present exciton model, the ground state wavefunction of the system Φ_0, consisting of N chromophores, can be written as a Hartree product, as no exchange of electrons between different chromophores are allowed, namely

$$\Phi_0 = \phi_1^0 \cdot \phi_\alpha^0 \ldots \phi_N^0 = \prod_\alpha^N \phi_\alpha^0 \tag{15}$$

where ϕ_α^0 is the ground state wavefunction of chromophore α. The excited state wavefunctions can be written in a similar fashion:

$$\Phi_\beta^J = \phi_1^0 \cdot \phi_\alpha^0 \ldots \phi_\beta^J \ldots \phi_N^0 = \phi_\beta^J \prod_{\alpha \neq \beta}^N \phi_\alpha^0 \tag{16}$$

where the notation Φ_β^J means that we consider the local electronic state on chromophore β in the excited state J in the diabatic representation of local excited states. For simplicity, we will only discuss the overlap between diabatic wavefunctions, as the adiabatic overlap matrix can be obtained afterwards from the corresponding diabatic one by a unitary transformation.

From the output of the QM calculation of the individual chromophores it is possible to construct their local wavefunction overlaps as:

$$\mathbf{S}_\alpha(t, t + \Delta t) = \begin{pmatrix} \langle \phi_\alpha^0 | \tilde{\phi}_\alpha^0 \rangle & \langle \phi_\alpha^0 | \tilde{\phi}_\alpha^1 \rangle & \cdots & \langle \phi_\alpha^0 | \tilde{\phi}_\alpha^M \rangle \\ \langle \phi_\alpha^1 | \tilde{\phi}_\alpha^0 \rangle & \langle \phi_\alpha^1 | \tilde{\phi}_\alpha^1 \rangle & \cdots & \langle \phi_\alpha^1 | \tilde{\phi}_\alpha^M \rangle \\ \vdots & \vdots & \ddots & \vdots \\ \langle \phi_\alpha^M | \tilde{\phi}_\alpha^0 \rangle & \langle \phi_\alpha^M | \tilde{\phi}_\alpha^1 \rangle & \cdots & \langle \phi_\alpha^M | \tilde{\phi}_\alpha^M \rangle \end{pmatrix} \tag{17}$$

here shown for a chromophore with M excited states. Once all chromophore overlaps are obtained it is straightforward to build the total overlaps of the excitonic model. The overlap term for the exciton ground state is given as

$$S_0(t, t + \Delta t) = \langle \Phi_0 | \tilde{\Phi}_0 \rangle = \prod_{\alpha}^{N} \langle \phi_\alpha^0 | \tilde{\phi}_\alpha^0 \rangle \tag{18}$$

The excited state wavefunction overlaps in the diabatic representation can be divided into two different cases: one between locally excited states on the same chromophore,

$$S_{\alpha,\alpha}^{IJ}(t, t + \Delta t) = \langle \Phi_\alpha^I | \tilde{\Phi}_\alpha^J \rangle = \langle \phi_\alpha^I | \tilde{\phi}_\alpha^J \rangle \prod_{\beta \neq \alpha}^{N} \langle \phi_\beta^0 | \tilde{\phi}_\beta^0 \rangle = \frac{\langle \phi_\alpha^I | \tilde{\phi}_\alpha^J \rangle}{\langle \phi_\alpha^0 | \tilde{\phi}_\alpha^0 \rangle} S_0(t, t + \Delta t) \tag{19}$$

and another between locally excited states on two different chromophores,

$$S_{\alpha,\beta}^{IJ}(t, t + \Delta t) = \langle \Phi_\alpha^I | \tilde{\Phi}_\beta^J \rangle = \langle \phi_\alpha^I | \tilde{\phi}_\alpha^0 \rangle \langle \phi_\beta^0 | \tilde{\phi}_\beta^J \rangle \prod_{\gamma \neq \beta, \alpha}^{N} \langle \phi_\gamma^0 | \tilde{\phi}_\gamma^0 \rangle = \frac{\langle \phi_\alpha^I | \tilde{\phi}_\alpha^0 \rangle}{\langle \phi_\alpha^0 | \tilde{\phi}_\alpha^0 \rangle} \frac{\langle \phi_\beta^0 | \tilde{\phi}_\beta^J \rangle}{\langle \phi_\beta^0 | \tilde{\phi}_\beta^0 \rangle} S_0(t, t + \Delta t) \tag{20}$$

The wavefunction overlap matrix in the diabatic exciton basis is set up using these terms for all involved states and is then transformed into the adiabatic basis to approximate the non-adiabatic couplings between the adiabatic states.

2.4 Wavefunction Analysis

The computed excited states were analysed using the TheoDORE[46] package to quantify their charge transfer character. Here, the central quantity is the one-electron transition density matrix $\mathbf{D}^{0\alpha}$ between the ground state and a specific exited state α defined as

$$D_{\mu\nu}^{0\alpha} = \langle \Phi_0 | \hat{a}_\mu^\dagger \hat{a}_\nu | \Phi_\alpha \rangle \tag{21}$$

where $\hat{a}_\mu^\dagger$ and $\hat{a}_\nu$ are the creation and annihilation operators pertaining to the atomic orbitals indexed μ and ν. For the analysis, the system was partitioned into two fragments

14

corresponding to the T4 and BOD units. Subsequently, the charge transfer numbers

$$\Omega_{AB}^{\alpha} = \frac{1}{2} \sum_{\mu \in A} \sum_{\nu \in B} \left[\left(\mathbf{D}^{0I} \mathbf{S} \right)_{\mu\nu} \left(\mathbf{S} \mathbf{D}^{0I} \right)_{\mu\nu} + D_{\mu\nu}^{0I} \left(\mathbf{S} \mathbf{D}^{0I} \mathbf{S} \right)_{\mu\nu} \right] \tag{22}$$

were computed, where A and B refer to any of the two fragments, $\mathbf{S}$ is the atomic overlap matrix, and the summations run over the basis functions located on the respective fragment. Hereby, diagonal elements $(A = B)$ represent local excitations on A, while off-diagonal elements show the individual charge transfer weights. Finally, the total charge transfer character (CT) can be defined as the sum of off-diagonal elements:

$$\text{CT} = \frac{1}{\Omega} \sum_{A \neq B} \Omega_{AB} \tag{23}$$

This CT value is discussed below. Further information can be found in Refs 47,48.

3 Computational Details

All electronic structure calculations were performed with Gaussian09[32] using DFT and its excited state variant, the linear response formulation of TDDFT. To ensure a good comparison with the work of Wiebeler et al. in Ref. 36 we chose the same functional and basis set namely CAM-B3LYP/6-31G(d). The MM calculations were also done with Gaussian 09 using its implementation of the AMBER force field.[49] The MM charges used for the electrostatic embedding were obtained from ESP fit[50] of the ground state density on the equilibrium structure of the individual chromophores using CAM-B3LYP/6-31G(d). The ESP charges were fitted to the heavy atoms (not hydrogen) of the system using 10 layers of grid points generated according to the Merz-Singh-Kollman scheme with a density of points per unit area of 10, as implemented in Gaussian09.[51,52]

Covalent bonds between the QM and MM regions are handled via the established link atom (LA) scheme (see Fig. 3):[53,54] for a given bond between QM atom Q1 and the MM

atom M1, the link atom is set at a fixed length from Q1 along the Q1-M1 bond, namely,

$$R(LA) = \vec{R}_{Q1} + \vec{R}_{M1-Q1} \frac{R_{Q1-LA}}{R_{Q1-M1}} \tag{24}$$

with R_{Q1-LA} being a fixed parameter that represents the average bond distance between Q1 and LA (e.g. for C-H bound it is 1.09 Å). To avoid the well known overpolarization problem in electrostatic embedding,[53–55] the default Z3 method[56] implemented in the Gaussian09 ONIOM scheme has been used, which puts the charges on M1, M2 and M3 atoms (see Fig. 3) to zero. Additionally any excess charge that might result from the Z3 scheme, is redistributed over all the other MM atoms.
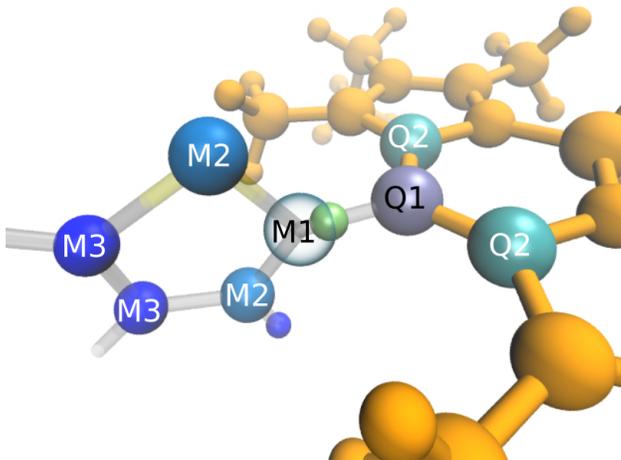

Figure 3: QM/MM setup for the BODT4, with BOD (orange) being the QM region and T4 (transparent) the MM region. The link atom (green) is placed on the Q1-M1 bond at a fixed distance. The eliminating charge method Z3 was used so that M1, M2 and M3 atoms do not bear a charge.

The 1000 initial conditions for the surface hopping dynamics were obtained from a Wigner distribution, using the frequencies and equilibrium structure of the full system at TDDFT level of theory. The absorption spectrum was computed from these 1000 structures, by applying a Gaussian broadening of 0.1 eV. Then, an excitation window was chosen at 3.3 eV with a width of 0.1 eV and the dynamics was performed using the here presented exciton method combined with the SHARC suite of codes.[33,34,57,58] The exciton model is based on

TMA couplings, but PDA couplings were also tested. For the calculation of the TMA couplings, the interaction between the Q1 atom on T4 and the M1 atom at the BOD moiety was screened with a redistributed charge and dipole scheme (rcd)[55,56] as the couplings at the boundary between the two fragments are overestimated due to the fact that the Q1 and M1 atoms are covalently bound and therefore very close to each other. For the PDA couplings the center of mass of the chromophores was chosen as the origin of the point dipoles and no further constrains were imposed. To account for the well-known overcoherence problem in surface hopping, we apply the energy-based decoherence correction by Granucci and Persico[59] (using C=0.1 H) to adjust the electronic coefficients at each time step.

4   Results and Discussion

To validate our implementation we chose as a test case the BODT4 molecular dyad shown in Fig. 1. The two fragments are only weakly coupled, as their wavefunction overlap is small due to the orthogonality of the conjugated moieties. The results of this work are finally compared to the experiments and the calculations performed by Wiebeler et al.[36] still using surface hopping dynamics but treating whole dyad at TDDFT level of theory.

4.1   Absorption spectra

As a first step, we took 1000 geometries obtained from a Wigner sampling of the full-QM system and computed the excitation energies of the first six excited states with the exciton model and with TDDFT on the whole system. Within the Franck-Condon region, in almost all cases, the TDDFT calculations on BODT4 show a S_1 state localized on the BOD moiety and a S_2 state localized on the T4 fragment. The S_3 and S_4 states instead appear strongly coupled and switch character frequently, with one being the CT state and the other the second locally excited state of the BOD. Considering that, by construction, the exciton model does not include CT states and therefore these states have to be excluded to allow for

a meaningful comparison. For this purpose, the excited states computed with full-QM were subjected to a preliminary check using the wavefunction analysis toolbox TheoDORE[46–48] to quantify their excited state CT character and states with CT value > 0.2 were eliminated from the analysis.

The root mean squared error with the full-QM values as reference is within $0.06 - 0.07$ eV for the two lowest states, with S_1 showing a slightly smaller error. For the S_3, the error is somewhat larger (0.1 eV), due to mixing of the CT state. From this comparison, we can therefore conclude that the exciton model is able to reproduce well the first two excited states of BODT4 while by construction it cannot describe CT states. However, the latter may be too low in energy, anyway, as the underestimation of energies of CT states is one of the known limitation of most TDDFT exchange-correlation functionals,[60] even if long-range corrected functionals are employed.

The UV absorption spectra calculated with the exciton and the full-QM methods are shown in Fig. 4 together with experimental spectrum (blue). The spectrum obtained with the exciton method was obtained within the TMA approximation (black), whereas for the full-QM model, two spectra are reported, one extracted from Ref. 36 (red, dashed) and one recalculated here (red, dotted) with the same spectral broadening used for the exciton model. All spectra show two dominant peaks. Using the exciton model, these are located around 460 nm and 360 nm. As it can be seen in the lower panel of Fig. 4, the first peak corresponds to the S_1 state of the system, dominated by the lowest singlet excitation of the BOD moiety. The second peak has strong contributions from both S_2 (localized on T4) and S_3. The full-QM spectra are slightly blue shifted in line with the RMSD error discussed before. On the other hand, all computed spectra are blue shifted compared to the experiments by about 0.45 eV, and in Fig. 4 the experimental spectrum has been shifted by this value for easier comparison. The main difference between the various computational spectra is the intensity ratio between the maxima of the two peaks. Interestingly, the best agreement with experiments, i.e. a lower intensity for the lower wavelength peak, is obtained

for the exciton model when compared either to the full-QM calculations of Ref. 36 or the full-QM calculations performed here. This suggests that the exciton model profits from error cancellation in this case.
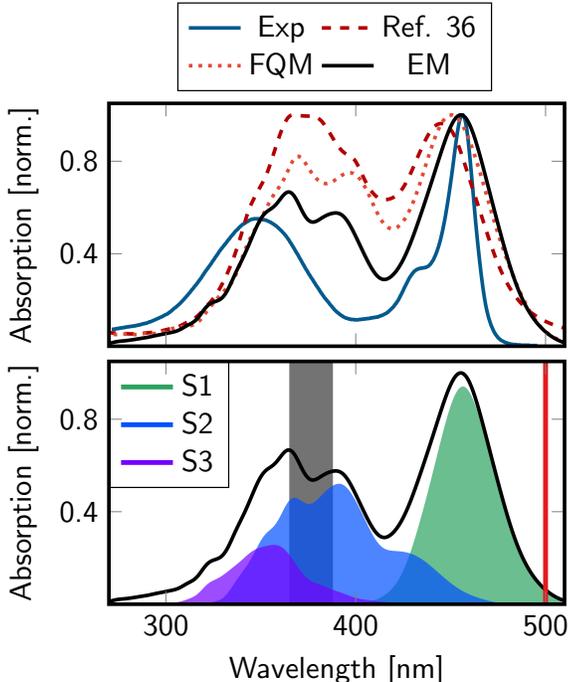

Figure 4: Upper Panel: absorption spectra of BODT4 calculated using the TMA exciton model (EM, black) on 1000 structures obtained from a Wigner sampling and the experimental results measured in cyclohexane (blue). The latter was blue shifted by 0.45 eV. Two full QM spectra are also reported: one taken from Ref. 36 (red dashed line) and one calculated using the same structures as for the exciton model (FQM, red dotted line). In the lower panel the EM spectrum is shown with the contributions of its first three excited states resolved. The excitation window (grey) and the probe wavelength (red) for the photoluminesence computations are also shown.

4.2 Dynamics

Experiments with a fluorescence upconversion technique[61] show ultrafast dynamics through the photoluminescence (PL) of BODT4 after photoexcitation.[36] We simulated this dynamics by performing surface hopping dynamics on the system using our exciton approach and compared with the results obtained experimentally and with the full-QM model, respectively.

19

4.2.1 Populations

For the excited state dynamics, an excitation window centered at 3.3 eV with a width of 0.1 eV was chosen, in agreement with the initial conditions of Ref. 36 and the experimental excitation wavelength after taking into account the blue shift between the computed and the excited spectrum. From the resulting 240 initial conditions within the excitation window, 174 were chosen randomly for the dynamics, with 144 starting in the S_2 and 30 in the S_3 state. The TMA exciton model dynamics shown in Fig. 5 (a) shows an ultrafast (within the first 120 fs) population transfer from the S_2 to the S_1. In contrast, the S_3 decays very little within 150 fs. The initial ultrafast population transfer from S_2 to S_1, as well as the rather constant population of S_3, are in good agreement with the full-QM results from Ref. 36, presented in Fig. 5 (c). The main difference between the full QM case and the exciton dynamics is that the initial ratio between S_2 and S_3 (+ S_4 for full-QM) population deviates for $t = 0$ fs. This can be explained mainly by the fact that the oscillator strength of the corresponding transitions are different between the exciton and the full-QM model. This difference was already evident in the spectra (see Fig. 4), which seemed to show a better behavior of the exciton model in reproducing the experimental findings. The second difference is that the exciton model has no initial population in the S_4, while around 12% of the full-QM population is in that state at the beginning of the dynamics. This is an artifact of the strong CT character of the S_3/S_4 state around the Franck-Condon region. As the CT state is missing in the exciton model, the S_4 state is instead a local excitation of the T4 moiety, higher in energy and therefore not populated.

For the first 100 fs we also computed another exciton dynamics using PDA couplings (see Fig. 5 (b)). Hereby we use only 99 trajectories. The two exciton dynamical studies (with TMA and PDA) show very similar results for the first 50 fs, namely the ultrafast S_2 to S_1 transition. The main difference between them is that the excitonic couplings between the S_1 on BOD and the S_1 on T4 are generally weaker in the dipole-dipole coupling scheme, due to the orthogonality of the transition dipole moments. This leads to a slower overall S_2-S_1
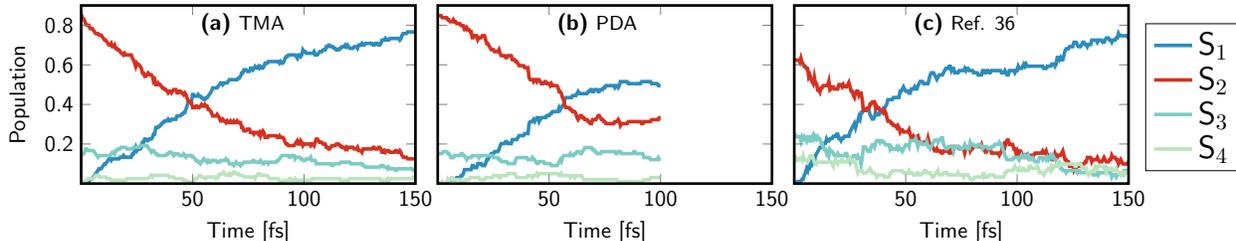
Figure 5: Classical populations for the exciton model with TMA (a) and the full-QM results (c) from Ref. 36 for the first 150 fs, while (b) shows the exciton results using PDA for 100 fs. The populations are shown in the adibatic picture for the first four excited state of the system.

transition and on the long run to a different equilibrium ratio of S_2 and S_1. While with TMA couplings the overall rise of population of the S_1 resembles very well the full QM results, the smaller couplings in the PDA scheme lead to a smaller equilibrium population in the S_1 of about 55% compared to the 75% in the TMA scheme and the full QM results. This inaccuracy of the PDA approach, can be expected as the point dipole approximation breaks down if the distance between two chromophores is small, however, it is also worth noting that the simple Förster dipole-dipole couplings are able to describe the essential features of the excited state dynamics of this complicated system.

Wiebeler et al. interpreted the S_2 - S_1 transition as an excitation energy transfer from the T4 to the BOD moiety, as the S_2 is in most cases a local excitation on BOD, while the S_2 is a local excitation on the T4 group. Furthermore, they analyzed the dynamics and came to the conclusion that the EET proceeds via the population of a CT state as an intermediate.[36] The exciton model shows a similar rate for the EET and also identifies the T4 group as the donor and the BOD as the acceptor, but it does not include CT states, by construction. Therefore, the underlying mechanism of the EET reaction between the exciton model and the full QM cases is different. In the full-QM results it was concluded that the population of a state with partial CT character is the essential step to couple the two fragments and enable the energy transfer. In contrast, the present excitonic calculations show that the same dynamics can be reproduced without the inclusion of CT states. This indicates that

21

the influence of the CT state on the total mechanism is less dominant than believed in first place and instead the main driving force are the Coulombic couplings.

One nice feature of the exciton model is that it is straightforward to identify the character of the excited states by performing a unitary transformation in the diabatic representation of localized excited states, which is achieved by using the matrix $\mathbf{U}$ from Eq. (6). These diabatic populations are shown in Fig. 6. The overall behavior between diabatic and adiabatic
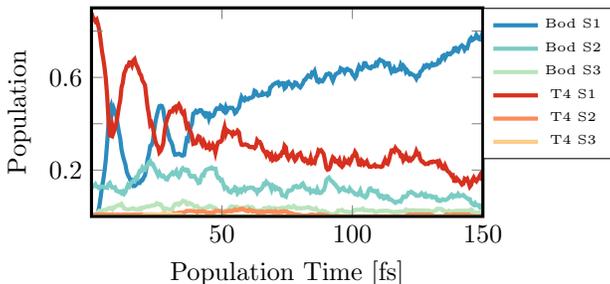

Figure 6: Diabatic populations through out the dynamics of the first three excited states of both BOD (blue) and T4 (red).

representations is similar. The system starts with almost all population in the S_1 on the T4 unit, which equals the S_2 of the total system and ends after 150 fs with most population in the S_1 of the system, which is localized on the BOD unit. A new feature that was not present in the adiabatic representation is that the population transfer between the two fragments is not a simple exponential decay, but instead shows ultrafast oscillations for the first 50 fs and it gets damped over time. These oscillations indicate that in the exciton picture the excitation energy is not transferred monotonically from T4 to BOD, but instead the excess energy oscillates between the two chromophores until the oscillations get damped and descend into an exponential transfer, similar to the one observed in the adiabatic picture.

4.2.2 Photoluminescence

The time-resolved PL spectrum was computed from the dynamics and compared with the experimental results in Ref. 36. Fig. 7 shows a 2D map of the frequency-dependent PL spectrum for the first 100 fs of the dynamics, with two specific energies, namely 500 nm

(red) and 380 nm (grey) highlighted. The latter wavelength corresponds to the excitation window illustrated in Fig. 4 and the former was chosen to match the experimental probe length of 600 nm in Ref. 36 accounting for the blue shift compared to the experimental results. The PL intensity was normalized in all cases to 1.0.
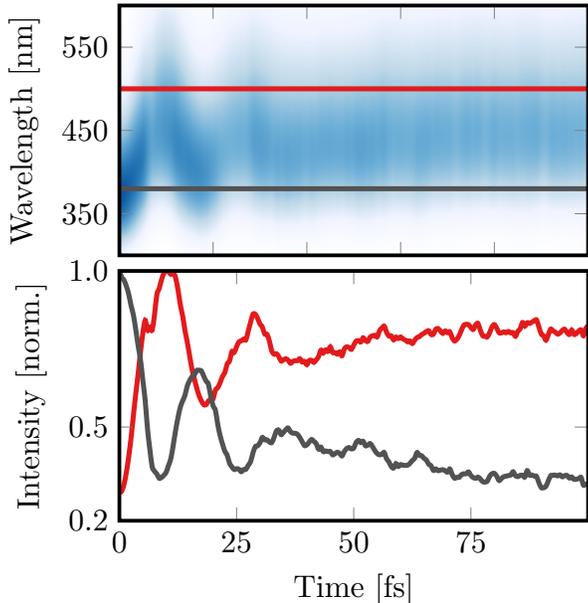

Figure 7: Calculated photoluminescence spectrum of the BODT4 dyad from the TMA exciton dynamics. The upper panel shows the results for the whole frequency spectrum, with the excitation window (380 nm, grey) and the probe wavelength (500 nm, red) highlighted. The lower panel shows the cuts along both wavelength.

For the probe wavelength we observe an ultrafast rise of intensity in the first 20 fs. At the excitation window the intensity shows an almost inverse behavior, indicating the population transfer from the Franck-Condon region. Interesting to note is that the PL spectra mirrors the populations in the diabatic picture, if the excitation window represents the S_1 on the T4 and the probe wavelength the S_1 on BOD (shown in Fig. 6) as discussed before. In particular, the ultrafast oscillation for the first 50 fs seconds is observed. The time-resolved PL was measured after an excitation at 425 nm, to excite primarily states localized at the T4 moiety and the results show as well a fast intensity increase with a rise-time of around 120 fs.[36] The time-resolution is unfortunately not high enough to resolve the ultrafast oscillations seen in Fig. 7. It would be interesting to investigate whether these oscillations could indeed

be resolved experimentally; however, the required time-resolution of about 10 fs poses a challenge.

5   Summary

We developed a QM/MM exciton model with electrostatic embedding for surface hopping dynamics of multichromophoric systems, including fully consistent excitation energies, gradients and non-adiabatic couplings obtained at TDDFT level of theory. Such a model has been obtained by interfacing the electronic structure code Gaussian for the computation of the individual chromophore properties and the surface hopping code SHARC.

As a proof of concept, we applied our model to a molecular dyad and compared the excitonic non-adiabatic dynamics with that obtained using a full QM surface hopping.[36] Although covalently bound systems are very challenging for exciton models, our results are in very good agreement with the full QM results, showing that the previously proposed mechanism going through a CT state is not necessary to obtain the same non-adiabatic dynamics and transfer times. A worse agreement is instead found when the point dipole approximation is used for the couplings, instead of the transition monopole approximation: the findings can be explained noting that the almost perpendicular orientation of the localized transition dipoles of the two moieties leads to an underestimation of their excitonic interaction.

An additional advantage of the proposed exciton model is that it is trivial to switch to the diabatic representation of local excited states to visualize the localization of the excitation on the individual chromophores throughout the dynamics. This makes it possible to see features that were not previously observed, namely ultrafast oscillatory energy transfer between the two fragments within the first 50 fs. The computed time-resolved PL spectrum shows also these ultrafast oscillations, as the oscillator strength of the individual exciton states depends strongly on the oscillator strength of the local excited states.

Acknowledgement

Supporting Information Available

The derivation of the subtractive QM/MM exciton scheme is presented in the SI in more detail. Additionally, we present a short benchmark on the computational costs, between TDDFT and our exciton model.

References

(1) Cheng, Y.-C.; Fleming, G. R. Dynamics of Light Harvesting in Photosynthesis. *Ann. Rev. Phys. Chem.* **2009**, *60*, 241–262.

(2) Scholes, G. D.; Mirkovic, T.; Turner, D. B.; Fassioli, F.; Buchleitner, A. Solar light harvesting by energy transfer: from ecology to coherence. *Energy Environ. Sci.* **2012**, *5*, 9374–9393.

(3) Schmidt, D.; Cho, Y. K. Natural photoreceptors and their application to synthetic biology. *Trends Biotechnol.* **2015**, *33*, 80–91.

(4) Kottke, T.; Xie, A.; Larsen, D. S.; Hoff, W. D. Photoreceptors Take Charge: Emerging Principles for Light Sensing. *Ann. Rev. Biophys.* **2018**,

(5) Markovitsi, D. Interaction of UV radiation with DNA. *Photochem. Photobio. Sci.* **2013**, *12*, 1256.

(6) Schreier, W. J.; Gilch, P.; Zinth, W. Early Events of DNA Photodamage. *Ann. Rev. Phys. Chem.* **2015**, *66*, 497–519.

(7) Gilbert, M.; Albinsson, B. Photoinduced charge and energy transfer in molecular wires. *Chem. Soc. Rev.* **2015**, *44*, 845–862.

(8) Kasha, M. Energy Transfer Mechanisms and the Molecular Exciton Model for Molecular Aggregates. *Radiat. Res.* **1963**, *20*, 55–70.

(9) You, Z.-Q.; Hsu, C.-P. Theory and calculation for the electronic coupling in excitation energy transfer. *Int. J. Quant. Chem.* **2013**, *114*, 102–115.

(10) Curutchet, C.; Mennucci, B. Quantum Chemical Studies of Light Harvesting. *Chem. Rev.* **2017**, *117*, 294–343.

(11) Hsu, C.-P.; Fleming, G. R.; Head-Gordon, M.; Head-Gordon, T. Excitation energy transfer in condensed media. *J. Chem. Phys.* **2001**, *114*, 3065–8.

(12) Iozzi, M. F.; Mennucci, B.; Tomasi, J.; Cammi, R. Excitation energy transfer (EET) between molecules in condensed matter: A novel application of the polarizable continuum model (PCM). *J. Chem. Phys.* **2004**, *120*, 7029–7040.

(13) Krueger, B. P.; Scholes, G. D.; Fleming, G. R. Calculation of Couplings and Energy-Transfer Pathways between the Pigments of LH2 by the ab Initio Transition Density Cube Method. *J. Phys. Chem. B* **1998**, *102*.

(14) Damjanović, A.; Ritz, T.; Schulten, K. Excitation transfer in the peridinin-chlorophyll-protein of Amphidinium carterae. *Biophys. J.* **2000**, *79*.

(15) Howard, I. A.; Zutterman, F.; Deroover, G.; Lamoen, D.; Van Alsenoy, C. Approaches to Calculation of Exciton Interaction Energies for a Molecular Dimer. *J. Phys. Chem. B* **2004**, *108*, 19155–19162.

(16) Madjet, M. E.; Abdurahman, A.; Renger, T. Intermolecular coulomb couplings from ab initio electrostatic potentials: Application to optical transitions of strongly coupled

pigments in photosynthetic antennae and reaction centers. *J. Phys. Chem. B* **2006**, *110*, 17268–17281.

(17) Förster, T. Zwischenmolekulare Energiewanderung und Fluoreszenz. *Ann. d. Phys.* **1948**, 55–75.

(18) Curutchet, C.; Muñoz-Losa, A.; Monti, S.; Kongsted, J.; Scholes, G. D.; Mennucci, B. Electronic Energy Transfer in Condensed Phase Studied by a Polarizable QM/MM Model. *J. Chem. Theory Comput.* **2009**, *5*, 1838–1848.

(19) Renger, T.; Müh, F. Understanding photosynthetic light-harvesting: a bottom up theoretical approach. *Phys. Chem. Chem. Phys.* **2013**, *15*, 3348–24.

(20) Scholes, G. D.; Curutchet, C.; Mennucci, B.; Cammi, R.; Tomasi, J. How Solvent Controls Electronic Energy Transfer and Light Harvesting. *J. Phys. Chem. B* **2007**, *111*, 6978–6982.

(21) Curutchet, C.; Scholes, G. D.; Mennucci, B.; Cammi, R. How Solvent Controls Electronic Energy Transfer and Light Harvesting: Toward a Quantum-Mechanical Description of Reaction Field and Screening Effects. *J. Phys. Chem. B* **2007**, *111*, 13253–13265.

(22) Neugebauer, J.; Curutchet, C.; Muñoz-Losa, A.; Mennucci, B. A Subsystem TDDFT Approach for Solvent Screening Effects on Excitation Energy Transfer Couplings. *J. Chem. Theory Comput.* **2010**, *6*, 1843–1851.

(23) Curutchet, C.; Kongsted, J.; Muñoz-Losa, A.; Hossein-Nejad, H.; Scholes, G. D.; Mennucci, B. Photosynthetic Light-Harvesting Is Tuned by the Heterogeneous Polarizable Environment of the Protein. *J. Am. Chem. Soc.* **2011**, *133*, 3078–3084.

(24) Moser, C. C.; Keske, J. M.; Warncke, K.; Farid, R. S.; Dutton, P. L. Nature of biological electron transfer. *Nature* **1992**, *355*, 796.

(25) Scholes, G. D.; Fleming, G. R.; Olaya-Castro, A.; van Grondelle, R. Lessons from nature about solar light harvesting. *Nat. Chem.* **2011**, *3*, 763–774.

(26) Nogueira, J. J.; Plasser, F.; González, L. Electronic delocalization, charge transfer and hypochromism in the UV absorption spectrum of polyadenine unravelled by multiscale computations and quantitative wavefunction analysis. *Chem. Sci.* **2017**, *8*, 5682–5691.

(27) Ishizaki, A.; Fleming, G. R. On the adequacy of the Redfield equation and related approaches to the study of quantum dynamics in electronic energy transfer. *J. Chem. Phys.* **2009**, *130*, 234110.

(28) Novoderezhkin, V. I.; van Grondelle, R. Physical origins and models of energy transfer in photosynthetic light-harvesting. *Phys. Chem. Chem. Phys.* **2010**, *12*, 7352–14.

(29) Chenu, A.; Scholes, G. D. Coherence in Energy Transfer and Photosynthesis. *Ann. Rev. Phys. Chem.* **2015**, *66*, 69–96.

(30) Sisto, A.; Glowacki, D. R.; Martinez, T. J. Ab Initio Nonadiabatic Dynamics of Multichromophore Complexes: A Scalable Graphical-Processing-Unit-Accelerated Exciton Framework. *Acc. Chem. Res.* **2014**, *47*, 2857–2866.

(31) Sisto, A.; Stross, C.; van der Kamp, M. W.; O'Connor, M.; McIntosh-Smith, S.; Johnson, G. T.; Hohenstein, E. G.; Manby, F. R.; Glowacki, D. R.; Martinez, T. J. Atomistic non-adiabatic dynamics of the LH2 complex with a GPU-accelerated ab initio exciton model. *Phys. Chem. Chem. Phys.* **2017**, *19*, 14924–14936.

(32) Frisch, M. J.; Trucks, G. W.; Schlegel, H. B.; Scuseria, G. E.; Robb, M. A.; Cheeseman, J. R.; Scalmani, G.; Barone, V.; Mennucci, B.; Petersson, G. A.; Nakatsuji, H.; Caricato, M.; Li, X.; Hratchian, H. P.; Izmaylov, A. F.; Bloino, J.; Zheng, G.; Sonnenberg, J. L.; Hada, M.; Ehara, M.; Toyota, K.; Fukuda, R.; Hasegawa, J.; Ishida, M.; Nakajima, T.; Honda, Y.; Kitao, O.; Nakai, H.; Vreven, T.; Montgomery, J. A.; Jr.,;

Peralta, J. E.; Ogliaro, F.; Bearpark, M.; Heyd, J. J.; Brothers, E.; Kudin, K. N.; Staroverov, V. N.; Kobayashi, R.; Normand, J.; Raghavachari, K.; Rendell, A.; Burant, J. C.; Iyengar, S. S.; Tomasi, J.; Cossi, M.; Rega, N.; Millam, J. M.; Klene, M.; Knox, J. E.; Cross, J. B.; Bakken, V.; Adamo, C.; Jaramillo, J.; Gomperts, R.; Stratmann, R. E.; Yazyev, O.; Austin, A. J.; Cammi, R.; Pomelli, C.; Ochterski, J. W.; Martin, R. L.; Morokuma, K.; Zakrzewski, V. G.; Voth, G. A.; Salvador, P.; Dannenberg, J. J.; Dapprich, S.; Daniels, A. D.; Farkas, .; Foresman, J. B.; Ortiz, J. V.; Cioslowski, J.; Fox, D. J. Gaussian 09 Revision D.01. 2009; Gaussian Inc. Wallingford CT.

(33) Richter, M.; Marquetand, P.; González-Vázquez, J.; Sola, I.; González, L. SHARC: ab initio Molecular Dynamics with Surface Hopping in the Adiabatic Representation Including Arbitrary Couplings. *J. Chem. Theory Comput.* **2011**, *7*, 1253–1258.

(34) Mai, S.; Marquetand, P.; González, L. A General Method to Describe Intersystem Crossing Dynamics in Trajectory Surface Hopping. *Int. J. Quantum Chem.* **2015**, *115*, 1215–1231.

(35) Mai, S.; Richter, M.; Heindl, M.; Menger, M. F. S. J.; Atkins, A.; Ruckenbauer, M.; Plasser, F.; Oppel, M.; Marquetand, P.; González, L. SHARC2.0: Surface Hopping Including Arbitrary Couplings - Program Package for Non-Adiabatic Dynamics. sharc-md.org, 2018.

(36) Wiebeler, C.; Plasser, F.; Hedley, G. J.; Ruseckas, A.; Samuel, I. D. W.; Schumacher, S. Ultrafast Electronic Energy Transfer in an Orthogonal Molecular Dyad. *J. Phys. Chem. Lett.* **2017**, *8*, 1086–1092.

(37) Barbatti, M. Nonadiabatic dynamics with trajectory surface hopping method. *Wiley Interdiscip. Rev. Comput. Mol. Sci.* **2011**, *1*, 620–633.

(38) Barbatti, M.; Ruckenbauer, M.; Plasser, F.; Pittner, J.; Granucci, G.; Persico, M.;

Lischka, H. Newton-X: a surface-hopping program for unadiabatic molecular dynamics. *WIREs: Comp. Mol. Sci.* **2014**, *4*, 26–33.

(39) Dapprich, S.; Komáromi, I.; Byun, K.; Morokuma, K.; Frisch, M. J. A new ONIOM implementation in Gaussian98. Part I. The calculation of energies, gradients, vibrational frequencies and electric field derivatives. *J. Mol. Struc.* **1999**, *461-462*, 1 – 21.

(40) Vreven, T.; Byun, K. S.; Komáromi, I.; Dapprich, S.; Montgomery, J. A.; Morokuma, K.; Frisch, M. J. Combining Quantum Mechanics Methods with Molecular Mechanics Methods in ONIOM. *J. Chem. Theory Comput.* **2006**, *2*, 815–826.

(41) Hammes-Schiffer, S.; Tully, J. C. Proton transfer in solution: Molecular dynamics with quantum transitions. *J. Chem. Phys.* **1994**, *101*, 4657–4667.

(42) Tapavicza, E.; Tavernelli, I.; Rothlisberger, U. Trajectory Surface Hopping within Linear Response Time-Dependent Density-Functional Theory. *Phys. Rev. Lett.* **2007**, *98*, 023001.

(43) Mitric, R.; Werner, U.; Bonacic-Koutecky, V. Nonadiabatic dynamics and simulation of time resolved photoelectron spectra within time-dependent density functional theory: Ultrafast photoswitching in benzylideneaniline. *J. Chem. Phys.* **2008**, *129*, 164118.

(44) Pittner, J.; Lischka, H.; Barbatti, M. Optimization of mixed quantum-classical dynamics: Time-derivative coupling terms and selected couplings. *Chem. Phys.* **2009**, *356*, 147 – 152.

(45) Plasser, F.; Ruckenbauer, M.; Mai, S.; Oppel, M.; Marquetand, P.; González, L. Efficient and Flexible Computation of Many-Electron Wavefunction Overlaps. *J. Chem. Theory Comput.* **2016**, *12*, 1207.

(46) Plasser, F. THEODORE: a package for theoretical density, orbital relaxation, and exciton analysis; available from `http://theodore-qc.sourceforge.net/`.

(47) Plasser, F.; Lischka, H. Analysis of Excitonic and Charge Transfer Interactions from Quantum Chemical Calculations. *J. Chem. Theory Comput.* **2012**, *8*, 2777–2789.

(48) Plasser, F.; Wormit, M.; Dreuw, A. New tools for the systematic analysis and visualization of electronic excitations. I. Formalism. *J. Chem. Phys.* **2014**, *141*, 0–13.

(49) Cornell, W. D.; Cieplak, P.; Bayly, C. I.; Gould, I. R.; Merz, K. M.; Ferguson, D. M.; Spellmeyer, D. C.; Fox, T.; Caldwell, J. W.; Kollman, P. A. A Second Generation Force Field for the Simulation of Proteins, Nucleic Acids, and Organic Molecules. *J. Am. Chem. Soc.* **1995**, *117*, 5179–5197.

(50) Singh, U. C.; Kollman, P. A. An approach to computing electrostatic charges for molecules. *J. Comput. Chem. 5*, 129–145.

(51) Chandra, S. U.; A., K. P. An approach to computing electrostatic charges for molecules. *J. Comput. Chem.* **1984**, *5*, 129–145.

(52) Besler, B. H.; Merz, K. M.; Kollman, P. A. Atomic charges derived from semiempirical methods. *J. Comput. Chem.* **1990**, *11*, 431–439.

(53) Senn, H. M.; Thiel, W. QM/MM Methods for Biomolecular Systems. *Angew. Chem. Int. Ed.* **2009**, *48*, 1198–1229.

(54) Groenhof, G. In *Biomolecular Simulations: Methods and Protocols*; Monticelli, L., Salonen, E., Eds.; Humana Press: Totowa, NJ, 2013; pp 43–66.

(55) Lin, H.; Truhlar, D. G. QM/MM: what have we learned, where are we, and where do we go from here? *Theor. Chem. Acc.* **2006**, *117*, 185.

(56) Lin, H.; Truhlar, D. G. Redistributed Charge and Dipole Schemes for Combined Quantum Mechanical and Molecular Mechanical Calculations. *J. Phys. Chem. A* **2005**, *109*, 3991–4004.

(57) Mai, S.; Richter, M.; Heindl, M.; Menger, M. F. S. J.; Atkins, A.; Ruckenbauer, M.; Plasser, F.; Oppel, M.; Marquetand, P.; González, L. SHARC2.0: Surface Hopping Including Arbitrary Couplings - Program Package for Non-Adiabatic Dynamics. sharc-md.org, 2018.

(58) Mai, S.; Marquetand, P.; González, L. Nonadiabatic Dynamics: The SHARC Approach. *WIREs Comput. Mol. Sci.* **2018**, in press.

(59) Granucci, G.; Persico, M.; Zoccante, A. Including quantum decoherence in surface hopping. *J. Chem. Phys.* **2010**, *133*, 134111.

(60) Dreuw, A.; Head-Gordon, M. Single-Reference ab Initio Methods for the Calculation of Excited States of Large Molecules. *Chem. Rev.* **2005**, *105*, 4009–4037.

(61) Hedley, G. J.; Ruseckas, A.; Samuel, I. D. Ultrafast luminescence in Ir(ppy)3. *Chem. Phys. Lett.* **2008**, *450*, 292 – 296.

Graphical TOC Entry